J. Fluid Mech. (2010), *vol.* 657, *pp.* 394–412. © Cambridge University Press 2010
doi:10.1017/S0022112010001424

Reynolds stress and eddy viscosity in direct numerical simulations of sheared two-dimensional turbulence

PATRICK F. CUMMINS† AND GREG HOLLOWAY

Institute of Ocean Sciences, Fisheries and Oceans Canada, 9860 W. Saanich Road, Sidney, BC, Canada V8L 4B2

(Received 11 February 2009; revised 15 March 2010; accepted 17 March 2010; first published online 10 June 2010)

The Reynolds stress associated with the adjustment of two-dimensional isotropic eddies subject to a large-scale shear flow is examined in a series of initial-value calculations in a periodic channel. Several stages in the temporal evolution of the stress can be identified. Initially, there is a brief period associated with quasi-passive straining of the eddy field in which the net Reynolds stress and the associated eddy viscosity remain essentially zero. In spectral space this is characterized by mutual cancellation of contributions to the Reynolds stress at high and low eddy wavenumbers. Subsequently, eddy–eddy interactions produce a tendency to restore isotropy at higher eddy wavenumbers, leading to an overall positive eddy viscosity associated with the dominant contribution to the Reynolds stress at low eddy wavenumbers. These results are consistent with theoretical predictions of positive eddy viscosity for initially isotropic homogeneous two-dimensional turbulence. Due to the inverse cascade, the accumulation with time of energy at the scale of the channel produces a competing tendency to negative eddy viscosity associated with linear shearing of the disturbances. This finite-domain effect may become dominant if the nonlinearity of the eddy field is relatively weak.

1. Introduction

Reynolds stresses mediate the exchange of momentum and energy between large-scale motions and turbulent eddies. An eddy viscosity may be defined based on a linear relation between the Reynolds stress tensor and the mean rate-of-strain tensor. In a strict sense, this definition requires the existence of a 'spectral gap', that is, the scale of the disturbances must be much smaller than the scale of variation of the background flow. In two-dimensional and quasi-geostrophic turbulence, a great many analytical and numerical studies (e.g. Fjortoft 1953; Kraichnan 1967; Fox & Orszag 1973), as well as geophysical and laboratory observations (Sommeria 1986), have demonstrated an inverse energy cascade involving the systematic transfer of eddy energy to larger scales. In a broad sense, the upscale spectral energy flux in two-dimensional turbulence may be regarded as a negative viscosity phenomenon (e.g. Starr 1968). However, the inverse cascade is associated with aggregation of like-signed vortices (e.g. Tabeling 2002) and occurs without a clear separation of spatial scales. Numerical studies of forced zonal flows in beta-plane channels calculate a

† Email address for correspondence: patrick.cummins@dfo-mpo.gc.ca

negative horizontal eddy viscosity (McWilliams & Chow 1981). Here as well, there is no spectral gap as the eddy scale is comparable to that of the channel. For certain anisotropic initial conditions, nonlinear theory (Gama, Vergassola & Frisch 1994) and numerical simulations (Benzi, Manfroi & Vergassola 1996; Chaves & Gama 2000) have demonstrated negative eddy viscosity in the absence of an externally imposed large-scale shear flow. On the other hand, in what might be regarded as a canonical problem, the sign of the eddy viscosity is not well established for two-dimensional turbulence in which a random sea of initially homogeneous isotropic eddies are subjected to a large-scale shear or strain flow.

Following Shepherd (1987) and Holloway (1989), the matter may be considered in terms of two distinct processes. The first is linear shearing of passive two-dimensional eddies by the large-scale flow. The second involves the influence of active eddies through their mutual interactions. If the root-mean-square (r.m.s.) eddy vorticity, ζ_{rms}, is much weaker than the background shear S, ($\zeta_{rms}/|S| \ll 1$), then eddy–eddy interactions will be weak. In this quasi-linear limit, an isotropic field of vortices is elongated and tilted by a shear flow. The dynamics are sometimes illustrated in terms of an initially circular vortex (e.g. Salmon 1998, figure 4.10) for which an up-gradient Reynolds momentum flux develops as the vortex is distorted by the shear flow; hence the eddy viscosity is negative and energy is transferred to the large-scale flow. The inference of negative viscosity based on consideration of an isolated vortex has been assumed to extend, in the quasi-linear limit, to a collection of small-scale vortices with zero net circulation (e.g. Eyink 2006). It has been argued that this process is an underlying physical mechanism for the inverse cascade (Chen *et al.* 2006).

In contradistinction to this view, Kraichnan (1976) showed that straining of a passive isotropic wave field produces no net change in the energy of the disturbances, implying that the eddy viscosity associated with this process is zero. Shepherd (1985) considered passive disturbances in shear and showed that they can either gain or lose energy depending on their initial spectral distribution. In the case of disturbances with no particular orientation, that is, for isotropic eddies, he found that the energy is invariant. In a complementary result, Holloway (1989) considered eddies in large-scale shear, allowing for low-order departure from isotropy, and found that no net stress developed.

The second process, involving turbulent eddy–eddy interactions, disrupts the linear shearing process and produces a tendency to isotropy on an eddy-turnaround time scale. Drawing on the closure theory of Herring (1975), Holloway (1989) pointed out that the tendency to restore isotropy should be more efficient at the high-wavenumber range of the eddy spectrum. The remaining anisotropy at lower eddy wavenumbers may be expected to produce a net stress with the sense of positive eddy viscosity. The speculative nature of this result was emphasized.

In the present paper, the sense of the eddy viscosity is examined in direct numerical simulations of uniformly sheared, initially isotropic two-dimensional turbulence in which there is a large spectral gap. There have been few calculations of this sort. The study of Toh, Ohkitani & Yamada (1991) focused largely on spectral transfers of enstrophy and the role of coherent vortices. Although Reynolds stress spectra were reported, the net stress and eddy viscosity were not discussed. Shepherd (1987) presented results from low-resolution simulations of non-uniformly sheared, beta-plane turbulence and found evidence for isotropization due to eddy–eddy interactions. The simulations provided indications of both positive and negative eddy viscosity.

Theory is reviewed in the next section. The numerical model and initial conditions are described in § 3. Results from inviscid and decaying numerical simulations are presented in § 4. A summary is given in § 5.

2. Review of theory

2.1. *Spectral theory*

In order to interpret the numerical results, it is useful to review briefly the theory of Holloway (1989). Assuming a Fourier expansion of the eddy vorticity, $\zeta(\boldsymbol{x}, t) = \sum \zeta_{\boldsymbol{k}} \exp(\mathrm{i}\boldsymbol{k}\cdot\boldsymbol{x})$, the unforced, inviscid evolution of the ensemble mean enstrophy spectrum, $Z_{\boldsymbol{k}} = \langle \zeta_{\boldsymbol{k}} \zeta_{-\boldsymbol{k}} \rangle$, in a large-scale plane Couette flow, $(U, V) = (Sy, 0)$, is given by

$$\frac{\partial Z_{\boldsymbol{k}}}{\partial t} - Sk_x \frac{\partial Z_{\boldsymbol{k}}}{\partial k_y} = T_{\boldsymbol{k}}. \tag{1}$$

Here (k_x, k_y) are components of the wave vector $\boldsymbol{k}$, $T_{\boldsymbol{k}}$ represents enstrophy tendencies associated with nonlinear interactions and angle brackets denote an ensemble mean. The spectrum becomes anisotropic due to the refraction by the background shear. Allowing only low-order departure from isotropy, an approximate representation of the spectrum, similar to one proposed by Herring (1975, equation (5)), is adopted,

$$2\pi k\, Z_{\boldsymbol{k}} = Z(k)\,[1 - P(k)\cos(2\phi_{\boldsymbol{k}}) - Q(k)\sin(2\phi_{\boldsymbol{k}})], \tag{2}$$

where $Z(k)\delta k$ represents the enstrophy in a band δk centred about scalar wavenumber $k = |\boldsymbol{k}| = \sqrt{k_x^2 + k_y^2}$, and $\phi_{\boldsymbol{k}}$ is the angle that $\boldsymbol{k}$ makes with the k_x axis. The functions, $P(k)$ and $Q(k)$, represent departure from isotropy and are assumed small compared to unity. The stress tensor may be expressed in terms of these functions as

$$\begin{pmatrix} \langle u^2 \rangle & \langle uv \rangle \\ \langle uv \rangle & \langle v^2 \rangle \end{pmatrix} = \frac{1}{2} \int E(k) \begin{pmatrix} 2 + P(k) & Q(k) \\ Q(k) & 2 - P(k) \end{pmatrix} \mathrm{d}k, \tag{3}$$

where $E(k) = Z(k)/2k^2$ is the energy spectrum. Development of a deviatoric stress thus depends on the production of $E(k)Q(k)$ by the shear acting on the eddy field.

A relation for $E(k)$ is obtained by substituting (2) into (1) and integrating over azimuthal angle $\phi_{\boldsymbol{k}}$. Equations for $E(k)P(k)$ and $E(k)Q(k)$ are obtained similarly, first multiplying by either $\cos(2\phi_{\boldsymbol{k}})$ or $\sin(2\phi_{\boldsymbol{k}})$, respectively, before integration. The result is a set of coupled equations for the evolution of the spectra,

$$\frac{\partial\, k^2 E(k)}{\partial t} + \frac{S}{8}\frac{\partial}{\partial k}\left(\frac{E(k)\,Q(k)}{k}\right) = T(k), \tag{4}$$

$$\frac{\partial\, E(k)\,P(k)}{\partial t} - \frac{S}{2}E(k)Q(k) = T_P(k), \tag{5}$$

$$\frac{\partial\, E(k)\,Q(k)}{\partial t} + \frac{S}{2}E(k)P(k) = T_Q(k) - \frac{S}{4}\frac{\partial\, kE(k)}{\partial k}. \tag{6}$$

The last term appearing in (6) is associated with Reynolds stress production by the shear. Assuming that $E(k)$ has a band-limited spectrum, then this production term changes sign at the peak of $k\,E(k)$. Thus, for $S > 0$, there will be a tendency to produce positive Reynolds stress ($-\langle uv \rangle > 0$) over the low-wavenumber portion of the eddy spectrum, and an opposing tendency for negative stress over the high-wavenumber range. If $kE(k)$ vanishes at high and low wavenumbers, then the net stress produced by the shear is zero. Although this result is apparently restricted to a low-order

representation of anisotropy according to (2), Holloway (2010) has shown that it is generally the case that, in the absence of nonlinear interactions, straining of initially isotropic disturbances produces no subsequent net stress. Likewise, it can be shown that the result of zero stress also holds for passive isotropic eddies subject to uniform shear.

The term $T_Q(k)$ appearing on the right-hand side of (6) represents transfers associated with eddy–eddy interactions. Based on closure theory (Herring 1975), this term may be expressed as

$$T_Q(k) = \int Q(l)K(k,l)\,\mathrm{d}l - \mu(k)\,Q(k) \approx -D(k)\,Q(k). \tag{7}$$

The two terms in the middle of (7) represent the spectral redistribution and decay of the anisotropy. Herring (1975, figure 7) has shown that these two terms may be approximated by the decay-like term on the right-hand side of (7) for which the coefficient $\partial D/\partial k > 0$, implying that decay of anisotropy is most efficient at large wavenumbers. This is intuitively appealing as nonlinear scrambling by eddies may be expected to restore isotropy most rapidly at the smallest scales. Given the form of the production term in (6) and an initial band-limited eddy spectrum, the decay of anisotropy is expected to be most pronounced over those scales associated with negative eddy viscosity.

2.2. *Finite-domain effects*

The processes governing the production and decay of the Reynolds stress spectrum appear as forcing terms on the right-hand side of (6). The second of these is associated with the linear shearing of disturbances. It was noted above that this term vanishes on integration, and thus makes no net contribution to the stress, provided that the energy spectrum is band-limited. This condition may hold for an initial ensemble of disturbances. However, in a finite domain it will be violated eventually as shear-induced spectral transfers and the inverse cascade fill the spectrum out to the lowest wavenumbers. Integrating (6) over wavenumber and making use of (3) and (7) we obtain

$$\frac{\mathrm{d}\,\langle uv\rangle}{\mathrm{d}t} + \frac{S}{4}\,\langle u^2 - v^2\rangle = -\frac{1}{2}\int_{k_0}^{k_{max}} D(k)\,Q(k)\,\mathrm{d}k + \frac{S}{8}k_0 E(k_0), \tag{8}$$

where the contribution $Sk_{max}\,E(k_{max})$ at the largest resolved wavenumber, k_{max}, has been assumed negligible. It is seen from (8) that accumulation of energy at the gravest wavenumber, k_0, produces a systematic tendency for a stress in the sense of negative eddy viscosity. This tendency competes with the opposing tendency of nonlinear interactions to suppress the high-wavenumber portion of the Reynolds stress spectrum that is associated with negative viscosity. The resulting net stress in a finite domain will depend on the time-dependent balance between these competing processes.

Finite-domain effects were recognized by Shepherd (1987, § 3.2) who noted that while in an infinite domain the energy is invariant for initially isotropic disturbances, 'when the spatial spectrum is discrete, however, then asymptotic decay must eventually prevail'. Under refraction of initially isotropic passive disturbances, energy losses at higher wavenumbers are balanced by energy gains at progressively lower wavenumbers. However, in a finite domain, the low-wavenumber bandwidth available to gain energy will be exhausted eventually. Subsequently, linear shearing is a process that acts in the sense of a negative viscosity on the disturbances.

3. Numerical model

The initial-value problem of a two-dimensional field of small-scale eddies embedded within a large-scale shear flow is considered with respect to the theory of § 2. The dynamics are governed by the vorticity equation,

$$\frac{\partial \zeta}{\partial t} + J(\psi, \zeta) = \nu \nabla^2 \zeta, \tag{9}$$

where ψ is a streamfunction such that the (x, y) components of velocity are given by $(u, v) = (-\partial\psi/\partial y, \partial\psi/\partial x)$. The vorticity, ζ, and streamfunction fields are related via the Poisson equation, $\nabla^2\psi = \zeta$. Equation (9) is integrated numerically in a periodic channel of dimensions $L \times L$, with the condition of no normal flow, $\psi = 0$, applied along sidewall boundaries at $y = \pm L/2$, and periodic boundary conditions in the x direction. Both inviscid ($\upsilon = 0$) and decaying experiments are considered.

The initial conditions for each model run are $\zeta(x, y, t = 0) = \zeta_e(x, y) - S$, where the zero mean random eddy component, ζ_e, is characterized by an r.m.s. vorticity, ζ_{rms}, and has a specified band-limited top-hat spectrum whose lower and upper wavenumber limits are given by (k_1, k_2), respectively. The constant $S > 0$ is the shear of the background flow, $U_0(y) = Sy$. Each numerical experiment consists of an ensemble of $N = 30$ runs with random initial eddy fields. Reducing the ensemble size from 30 to 15 members leads to only minor quantitative changes to ensemble means and standard deviations, indicating that the results are statistically robust. In the following, 95 % confidence intervals on estimated means are calculated using standard methods (e.g. von Storch & Zwiers 1999 § 5.4.4) based on the t-distribution with $N - 1$ degrees of freedom.

The evolution according to (9) includes straining of the eddy field by the background shear flow, as well as nonlinear eddy–eddy interactions. To isolate the influences of these processes on the Reynolds stress, experiments were conducted in which eddy interactions are omitted. These cases involve the advection of passive disturbances by the background flow according to the linearized inviscid vorticity equation,

$$\frac{\partial \zeta}{\partial t} + J(\psi_0, \zeta) = 0 \tag{10}$$

with $\psi_0(y) = (S/8)(L^2 - 4y^2)$. Ensemble runs with (10) make use of initial eddy fields that are identical to those for (9), allowing a direct comparison with nonlinear simulations and an examination of the influence of eddy–eddy interactions on the Reynolds stress.

The finite difference model is similar to that of Cummins & Holloway (1994), modified for cyclic boundary conditions in the x direction. It makes use of the energy and enstrophy conserving scheme of Arakawa (1966) to discretize the Jacobian operator in (9) and (10). In the inviscid experiments, the vorticity equation is integrated on the channel sidewalls using one-sided Arakawa operators (cf. Wang & Vallis 1994). A leap frog scheme is used for the time stepping with occasional application of the Huen scheme to prevent the development of a computational mode. The frictional term on the right-hand side of (9) is lagged one time step to maintain stability (e.g. Holland 1978). The FISHPACK routine HWSCRT (Swarztrauber & Sweet 1975) is used to solve the Poisson equation in the channel geometry. Except where noted, the results discussed below are drawn from integrations on a grid of dimensions $2048\,\Delta s \times 2048\,\Delta s$, with Δs the uniform lateral resolution. These results are representative of an extensive set of experiments that were conducted with varying

resolution, grid Reynolds number, initial spectral shape and a broad range of the nonlinearity parameter, $\zeta_{rms}/|S|$.

In the simulations, the disturbances undergo a transient evolution from their initial conditions that may involve an exchange of energy with the average along-channel flow, the sense of which depends on the sign of the net Reynolds stress. Neglecting friction, the evolution of the average flow, $\bar{u}(y,t)$, is related to the divergence of the Reynolds stress as $\partial\,\bar{u}/\partial t = -\partial\,\overline{u'v'}/\partial y$, with the overbar denoting an average in the (along-channel) x direction, and primes the deviation thereof. The mean flow kinetic energy, $E_Z = L^{-1}\int(\bar{u}^2/2)\,\mathrm{d}y$, and the eddy kinetic energy, $E_{KE} = L^{-1}\int \frac{1}{2}(\overline{u'^2 + v'^2})\,\mathrm{d}y$, vary inversely as

$$\frac{\mathrm{d}E_Z}{\mathrm{d}t} = -\frac{\mathrm{d}E_{KE}}{\mathrm{d}t} = L^{-1}\int \overline{u'v'}(\partial\bar{u}/\partial y)\,\mathrm{d}y.$$

The eddy viscosity is defined as $\upsilon_e(y) = -\overline{u'v'}(\partial\bar{u}/\partial y)^{-1}$. Assuming that the background shear is approximately constant, $\partial\,\bar{u}/\partial y \approx S > 0$, which is the case in the simulations, then energy is transferred from the mean flow to the eddies if the net Reynolds stress is positive, $R \equiv L^{-1}\int -\overline{u'v'}\,\mathrm{d}y > 0$. The overall eddy viscosity, $M = L^{-1}\int \upsilon_e\,\mathrm{d}y \approx S^{-1}R$, is positive in this circumstance and $\mathrm{d}E_{KE}/\mathrm{d}t \approx S^2 M > 0$.

4. Results

In the following, quadratic quantities such as the Reynolds stress and eddy kinetic energy are non-dimensionalized by twice the initial eddy kinetic energy, $2E_{KE}|_{t=0}$. Time is non-dimensionalized according to an advection time scale, $|S|^{-1}$, as this is the natural time scale for wave–mean flow interactions and shear-induced spectral transfers. The eddy turnaround time, $\tau_e = \zeta_{rms}^{-1}$, is also mentioned as this provides the natural time scale for eddy–eddy interactions.

The ideal experiment would be one in which unbounded homogeneous isotropic eddy fields are subject to a uniform shear flow. To approximate this situation, ensembles of initial fields are specified for which the characteristic eddy length scale is small compared to the dimensions of the channel domain. Accordingly, the wavenumber spectrum of the initial eddy fields is such that $(k_1, k_2) = (40, 60)$. Thus, there is initially a large spectral gap and the turbulence is essentially homogeneous, except in the immediate proximity of the channel sidewalls. It is recognized, however, that given the inverse cascade the influence of the finite-domain size will increasingly be felt as time advances, and the spectral gap between the background flow and the disturbances will vanish eventually.

4.1. *Inviscid simulations*

To focus on the role of nonlinearity in the evolution of the Reynolds stress, experiments in which the disturbances undergo an inviscid adjustment are considered first. Due to the forward cascade of enstrophy, the inviscid evolution leads to a build-up of variance at the grid scale and a tendency to enstrophy equipartition spectra (Salmon 1998). The simulations are terminated well before such a state is realized. As the accumulation of grid-scale variance is an artefact of inviscid dynamics, the sensitivity of the results to the treatment of small-scale motions is examined in a series of decaying experiments that include explicit viscous damping. These cases are discussed in § 4.2.

4.1.1. *Reference experiment*

The reference experiment is a strongly nonlinear one in the sense that the ratio of the r.m.s. eddy vorticity to the background shear is large, $\zeta_{rms}/|S| = 10$. The

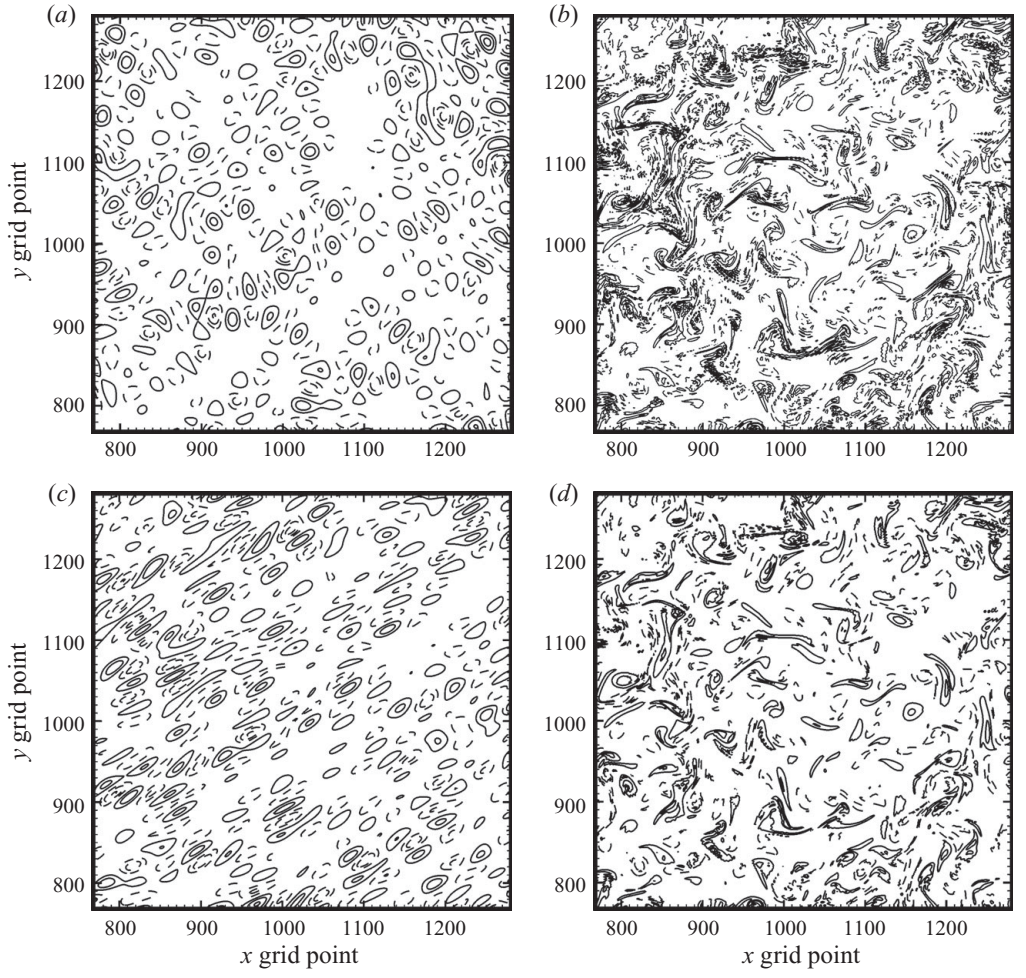

FIGURE 1. Inner portion of the eddy vorticity field from one member of the ensemble of the reference experiment at (*a*) $t=0$, and (*b*) $t=1.1$. (*c*) Eddy vorticity field at $t=1.1$ from the linearized experiment (§4.1.2). (*d*) Eddy vorticity from a decaying experiment (§4.2), also at $t=1.1$. The contour interval is ζ_{rms}, based on the r.m.s. vorticity at $t=0$. Solid lines denote positive values, dashed lines negative. The zero contour has been suppressed.

reason for this choice is to minimize the relative importance of finite-domain effects. Comparison with a corresponding linear experiment is given in §4.1.2, and variations in the parameter $\zeta_{rms}/|S|$ are considered in §4.1.3.

Figure 1(*a*) presents the vorticity field from one member of the ensemble of initial eddy fields of the reference experiment. (Only the innermost portion of the grid is shown for clarity.) Following release from the initial conditions, and after several eddy-turnaround time units ($\tau_e=11$), the vorticity field comes to be dominated visually by fine-scale filamentary vortex structures (figure 1*b*). The coherent elongation of the vortices by the shear flow is largely obscured, as might be expected for a case with strong eddy–eddy interactions. At subsequent stages in the flow evolution, the vorticity becomes dominated visually by a fine grain structure associated with an accumulation of grid-scale enstrophy.

Ensemble mean eddy kinetic energy spectra, $E(k)$, were computed by summing $\langle(k^2\psi'_{\boldsymbol{k}}\,\psi'_{-\boldsymbol{k}})/2\rangle$ over shells of constant k, where $\psi'_{\boldsymbol{k}}$ denotes the Fourier-transformed

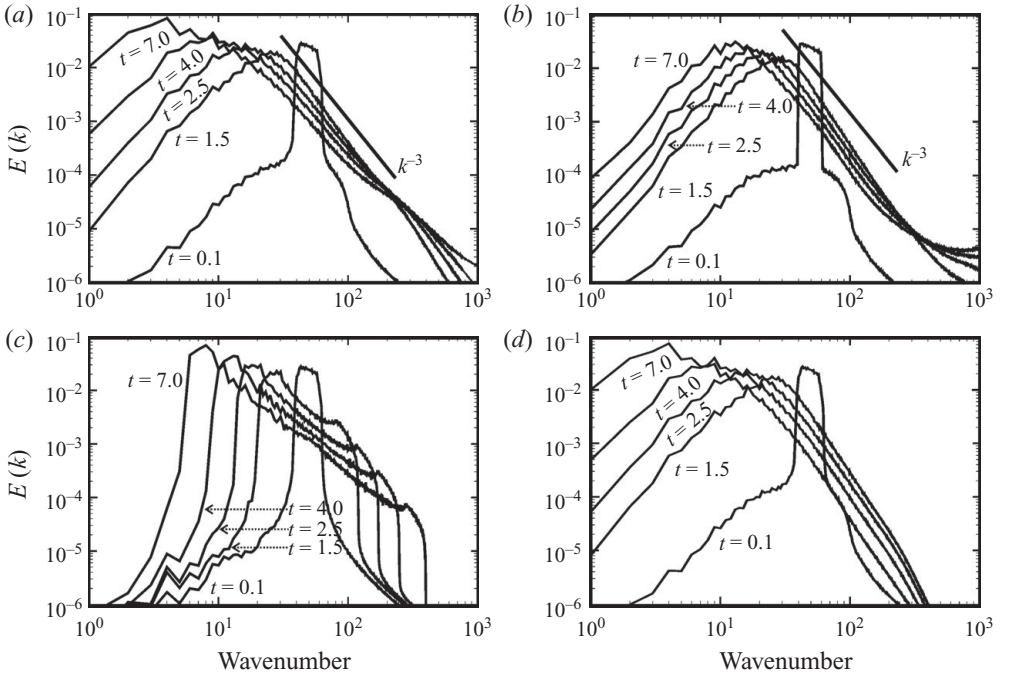

FIGURE 2. (*a*) Ensemble mean energy spectra, $E(k)$, at different times in the reference experiment ($\zeta_{rms}/|S| = 10$). (*b*) As in (*a*), but from an experiment in which the background shear is omitted ($S = 0$). (*c*) $E(k)$ for the linear experiment of § 4.1.2. (*d*) $E(k)$ for the decaying case of § 4.2 with $\zeta_{rms}/|S| = 10$ at $t = 0$.

eddy streamfunction. During the first few advection time units, the eddy scale is small compared to the domain size and the turbulence is essentially homogeneous, except in the immediate proximity of the channel boundaries. While the inhomogeneity in the y direction can lead to 'leakage' between spectral bands, this difficulty may be alleviated by tapering the eddy streamfunction in the proximity of the boundaries (von Storch & Zwiers 1999, § 12.3.8). However, as these fields vanish at the channel sidewalls, periodic extension of the streamfunction is not associated with a jump discontinuity (although derivatives may be discontinuous), and it was found that tapering had very little affect on the shape of the spectra. Accordingly, this step was omitted.

Figure 2(*a*) presents $E(k)$ at different times through the reference experiment. At stages through the temporal evolution, a k^{-3} scaling is evident in the spectra of figure 2(*a*), consistent with the development of an enstrophy inertial subrange. As expected, the spectral gap between the shear flow and eddy field collapses as eddy energy is transferred to the channel scale over a few advection time units. A comparison with spectra from a similar nonlinear experiment that omits the background shear (figure 2*b*) shows clearly that the presence of the shear speeds up appreciably the transfer of energy to the largest scales. This occurs as the shear-induced spectral transfer of energy to lower wavenumbers (Shepherd 1987, § 3) assists the inverse cascade to close the spectral gap.

The time variation of the ensemble mean net Reynolds stress, $\langle R \rangle$, along with 95 % confidence limits on the mean, are presented for the reference experiment in figure 3(*a*). At the outset of integration, $\langle R \rangle = 0$ for a brief period lasting somewhat less than half an eddy-turnaround time unit. Subsequently, the ensemble mean

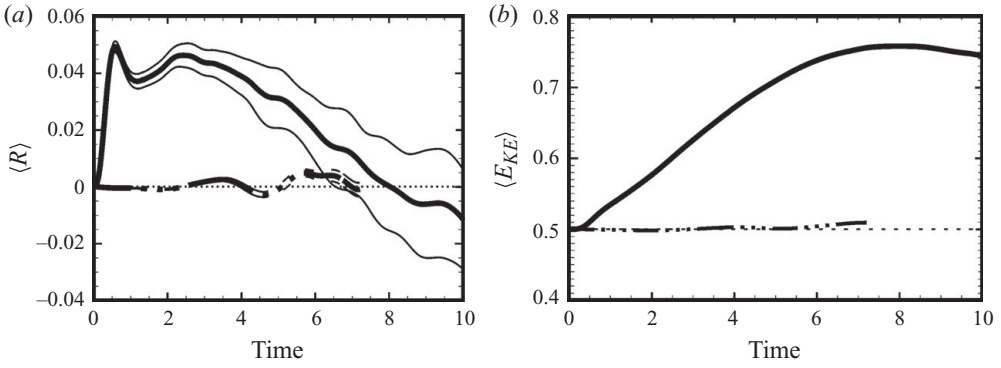

FIGURE 3. (*a*) Time variation of the ensemble mean net Reynolds stress, $\langle R \rangle$, from the reference experiment (thick solid line). Thin solid lines represent the 95 % confidence interval on the mean. The dashed-dotted lines are the ensemble mean and confidence interval for the linear experiment (§ 4.1.2). (*b*) Ensemble mean eddy kinetic energy, $\langle E_{KE} \rangle$, from the reference experiment (solid line), and from the linearized case (dashed-dotted line).

Reynolds stress increases rapidly to assume statistically significant positive values. Starting at about $t = 4$, the positive Reynolds stress begins to relax to zero within a gradually widening confidence interval as eddy energy accumulates at the largest scales (figure 2*a*). The results of figure 3(*a*) indicate a statistically robust positive eddy viscosity phenomenology for initially isotropic two-dimensional turbulence subject to a large-scale shear flow.

The ensemble mean eddy kinetic energy, $\langle E_{KE} \rangle$, is presented in figure 3(*b*). Consistent with zero initial Reynolds stress, the eddy kinetic energy remains constant for a brief period at the start of the integration. Subsequently, $\langle E_{KE} \rangle$ increases to over 50 % of its initial value. This increase is balanced by a compensating decrease in the kinetic energy of the mean flow (not shown) such that the total energy, $\langle E_{KE} + E_Z \rangle$, is constant. (The latter is conserved to within a factor of 10^{-5} over the course of the experiment.) Since $\langle E_Z \rangle \gg \langle E_{KE} \rangle$, the increase in eddy kinetic energy barely affects the along-channel mean flow which remains close to its initial linear cross-channel variation throughout the experiment. Small, but statistically significant, deviations occur within an eddy length scale of the channel sidewalls, where there is a stress divergence due to the condition of no normal flow. The energy balance of the ensemble is then well approximated by $\mathrm{d}\langle E_{KE} \rangle / \mathrm{d}t \approx S \langle R \rangle$. Accordingly, $\langle E_{KE} \rangle$ begins to decrease at about $t = 8$, in association with the change in the sign of $\langle R \rangle$.

The x-averaged ensemble mean Reynolds stress, $\langle -\overline{u'v'} \rangle$, shown in the Hovmüller (y–t) diagram of figure 4, provides an additional perspective on the spatial distribution and variability of the Reynolds stress. The diagram shows that during the first few advection time units the x-averaged Reynolds stress is almost uniformly positive across the channel. However, a boundary influence associated with negative Reynolds stress is apparent and gradually encroaches into the interior of the channel. This occurs as the scale of eddies located in the proximity of the boundary increases. Eventually, there is a fairly complete collapse of the positive Reynolds stress regime across the domain at about $t = 7$–8. This occurs as eddy energy accumulates at the scale of the channel and effects of the finite domain are felt. By this time, the initial spectral gap has largely closed (figure 2*a*).

One-dimensional Reynolds stress spectra, $-uv(k)$, permit a more detailed view of eddy–mean flow interactions. These spectra were compute by shell integration of

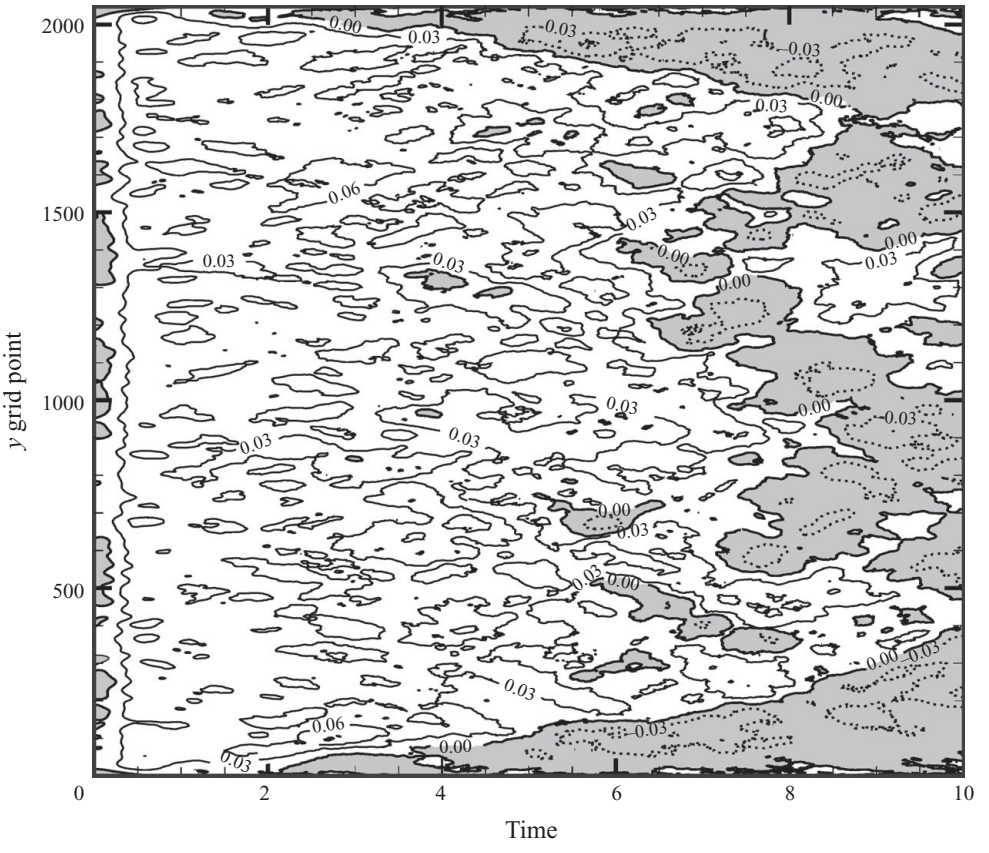

FIGURE 4. Hovmüller (y–t) diagram of the ensemble mean x-averaged Reynolds stress, $\langle -\overline{u'v'} \rangle$, from the reference experiment. Shading and dotted contours depict regions of negative Reynolds stress. The contour interval is 0.03.

$-uv_{\boldsymbol{k}} = \langle k_x k_y \psi'_{\boldsymbol{k}} \psi'_{-\boldsymbol{k}} \rangle$. Here as well, tapering the eddy streamfunction in the proximity of the channel boundaries has essentially no effect on the shape of the spectra and was omitted. The ensemble mean net Reynolds stress is then given by $\langle R \rangle = \int -uv(k)\,\mathrm{d}k$. Figure 5 presents $-uv(k)$, along with 95 % confidence intervals on the ensemble mean, at different times through the reference experiment. As the initial conditions are isotropic, $-uv(k) = 0$ at $t = 0$. Mean flow shearing of the eddy fields leads to opposing contributions to the Reynolds stress with positive (negative) values over the low (high) eddy wavenumber band. This is in accordance with the form of the anisotropy source term, $(S/4)(\partial\, kE(k)/\partial k)$, appearing in (6). The very early stages of the experiment are characterized by a mutual cancellation of these contributions (figure 5*a*) such that the net stress is essentially zero. At a somewhat later time (figure 5*b*), $-uv(k)$ is dominated by the positive contribution at lower wavenumbers, consistent with the development of a net positive Reynolds stress and positive eddy viscosity (figure 3*a*). This persists as the dominant contribution to $-uv(k)$ shifts continuously to lower wavenumbers (figure 5*c*). Towards the end of the simulation, the only non-zero contributions to the mean Reynolds stress spectra are concentrated at the lowest wavenumbers and lie within a wide confidence interval (figure 5*d*).

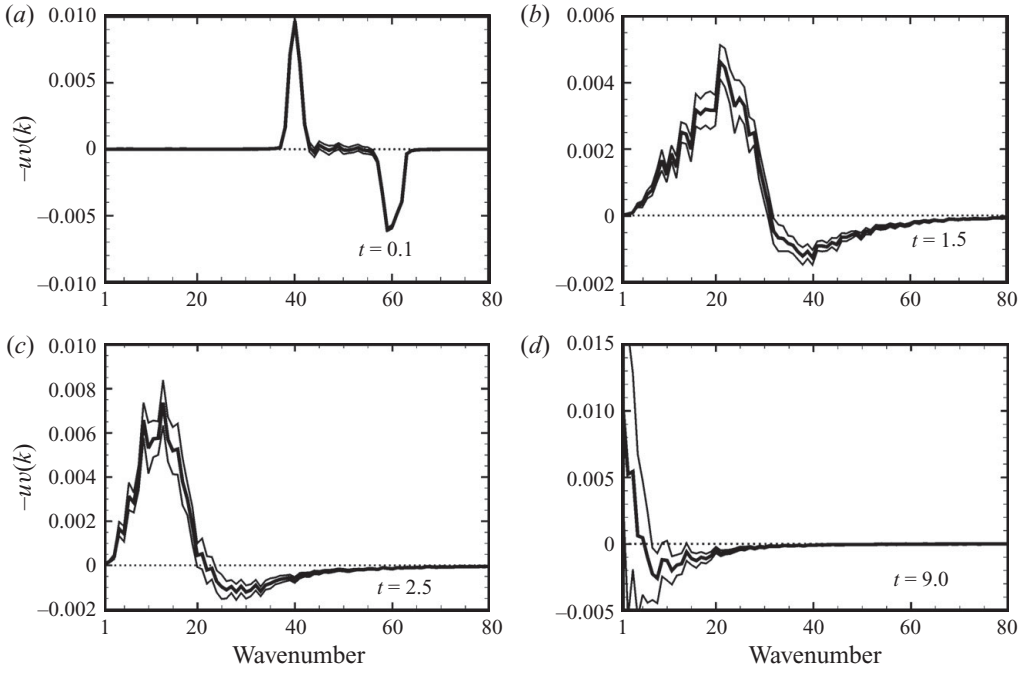

FIGURE 5. Ensemble mean Reynolds stress spectra, $-uv(k)$ (thick lines), and 95 % confidence interval (thin lines) at different times through the reference experiment.

4.1.2. *Linear experiment*

A companion experiment to the reference case was conducted in which the linearized advection equation (9) was integrated. The initial conditions for this experiment consist of the same eddy fields as for the reference experiment. However, as turbulent interactions are suppressed, the linear case amounts effectively to the parameter choice, $\zeta_{rms}/|S| = 0$. The individual runs for the linear case were integrated forward for seven advection time units, which was sufficient to compare with the reference case. Figure 1(c) shows the eddy vorticity field from one member of the ensemble. The elongation and rotation of eddies by the mean flow is evident here. Energy spectra from the linear case (figure 2c) show a progressive transfer to larger scales associated with the shear-induced spectral transfer. However, due to the absence of the inverse cascade, the accumulation of energy at the largest scales proceeds much more slowly than in the nonlinear cases.

Passive straining or shearing of isotropic, homogeneous disturbances yields zero net stress for all time (Holloway 2010). However, due to the presence of the sidewalls, the eddy fields of the simulations are not strictly homogeneous or isotropic and, as a result, non-zero Reynolds stresses may ensue. The time variation of the ensemble mean stress from the linear counterpart to the reference experiment is included in figure 3(a). This shows the slow development of weak values of $\langle R \rangle$ that are of variable sign and small in magnitude compared with those of the nonlinear case. Consistently, the eddy kinetic energy of the linear experiment remains nearly invariant, as seen in figure 3(b). These contrasting results indicate that nonlinear interactions are essential in producing the positive Reynolds stress and eddy viscosity seen in the reference experiment.

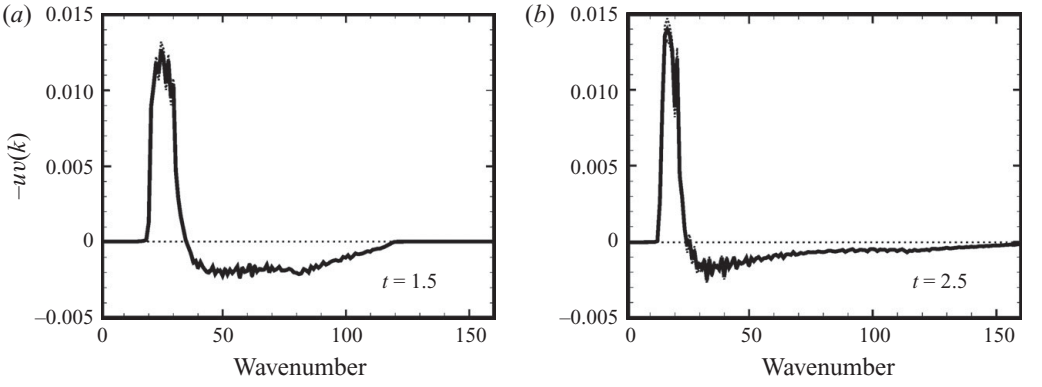

FIGURE 6. Ensemble mean Reynolds stress spectra, $-uv(k)$, from the linear counterpart to the reference experiment (§ 4.1.2). The 95 % confidence interval, plotted as thin lines, is barely evident due to the small statistical variability in this case. The horizontal axis is expanded in comparison with the spectra of figure 5.

Reynolds stress spectra from the linear case are shown in figure 6 and provide a point of comparison with the spectra of figure 5. Near the outset of the run, the $-uv(k)$ spectrum (not shown) is similar to that of figure 5(a), with nearly symmetric and mutually cancelling contributions at high and low eddy wavenumbers. In contrast to the nonlinear reference experiment, this mutual cancellation is largely maintained through subsequent stages of the evolution such that the resulting net stress remains very small. Specifically, the areas below and above the horizontal axes in figure 6(a, b) balance to within approximately 1 %. With the advance of time, the contribution to positive Reynolds stress shifts to the left and becomes increasingly concentrated within a small range of low wavenumbers, while the negative Reynolds stress contribution spreads to increasingly higher wavenumbers. Comparing the spectra of figure 5(b, c) with those of figure 6(a, b), it is evident that the eddy–eddy interactions present in the reference experiment eliminate the contribution to the stress at higher wavenumbers. This permits the development in the reference case of a net positive stress due to the dominant contribution at low wavenumbers, in accordance with the theory outlined in § 2.

The spectral distribution of the Reynolds stress in figure 6 can be understood in terms of wave refraction. In the absence of nonlinear interactions and dissipation, the enstrophy spectrum $Z_{\boldsymbol{k}}$ is conserved as the wave vector $\boldsymbol{k}$ is refracted by the shear flow, $U_0(y) = Sy$, according to $\mathrm{d}\boldsymbol{k}/\mathrm{d}t = (0, -Sk_x)$. The time variation of the wavenumber components is then $(k_x, k_y) = (k_x^0, k_y^0 - Sk_x^0 t)$, where (k_x^0, k_y^0) are initial values. The evolution is illustrated schematically in figure 7(a) for an isotropic initial distribution along $|\boldsymbol{k}| = (k_1 + k_2)/2 = 50$. Waves found at a given time in the upper quadrant ($k_x \cdot k_y > 0$) are oriented such that $\langle -u'v' \rangle > 0$ and extract momentum and energy from the mean flow as they are refracted. Conversely, waves whose wavenumber vector lies in the lower quadrant ($k_x \cdot k_y < 0$), for which $\langle -u'v' \rangle < 0$, give up energy to the mean flow. For isotropic initial conditions, these opposing tendencies exactly balance, resulting in zero net stress. As time progresses, wavenumber vectors lying in the upper quadrant become confined to increasingly smaller magnitudes, while the opposite occurs in the lower quadrant. It is this process that accounts for the progressive concentration, evident in figure 6(a, b), of positive Reynolds stress at low wavenumbers, while the negative Reynolds stress spreads to increasingly large wavenumbers.

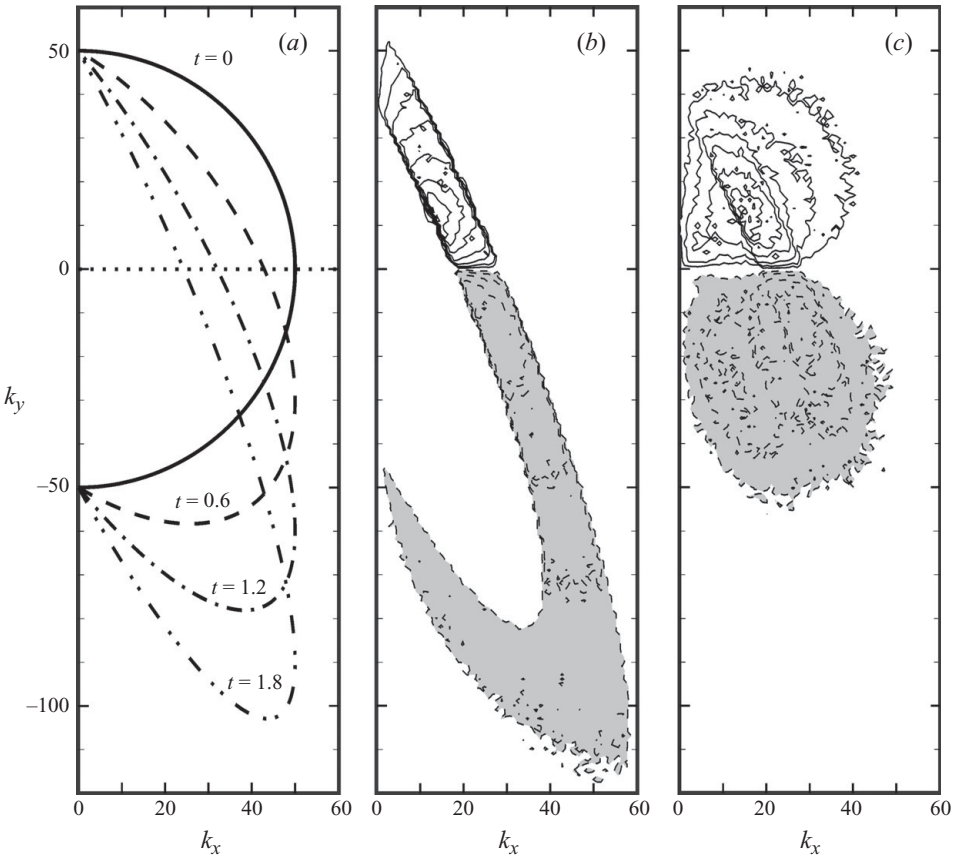

FIGURE 7. (*a*) Evolution of two-dimensional enstrophy spectra under shear flow refraction. Time is scaled by the shear. At $t = 0$, enstrophy variance is uniformly distributed along a circle in the (k_x, k_y) plane. (*b*) Ensemble mean two-dimensional Reynolds stress spectrum from the linear experiment (§ 4.1.2) at $t = 1.8$. Negative contours are dashed and shaded. (*c*) As in (*b*), but for a case with moderate nonlinearity, $\zeta_{rms}/|S| = 5$ at $t = 1.8$. Identical contours are drawn in (*b*) and (*c*).

Taking into account the finite spectral bandwidth of the initial disturbances, ensemble mean two-dimensional Reynolds stress spectra, $-uv_{\boldsymbol{k}}$, from the linear experiment (e.g. figure 7*b*) are consistent with simple wave refraction. With the inclusion of nonlinearity (figure 7*c*) the shear-induced spectral transfer is disrupted by the process of isotropization, that is by the redistribution of disturbance enstrophy and energy along contours of constant $|\boldsymbol{k}|$. This is especially effective at large $|k_y|$, thus allowing the positive stress contribution at smaller wavenumbers to emerge dominant. Also clearly evident in figure 7(*c*) is the nonlinear transfer across contours of $|\boldsymbol{k}|$ leading, in particular, to excitation of the gravest wavenumbers.

Under wave refraction, the net cancellation of positive and negative contributions to the Reynolds stress is maintained as time advances. However, in a finite domain, for which the spectrum is discrete, a state will be reached eventually such that the bandwidth in the upper quadrant is exhausted and it is no longer possible for waves at low wavenumbers to gain energy and balance the losses occurring at high wavenumbers. Subsequently, the contribution at large wavenumbers dominates and

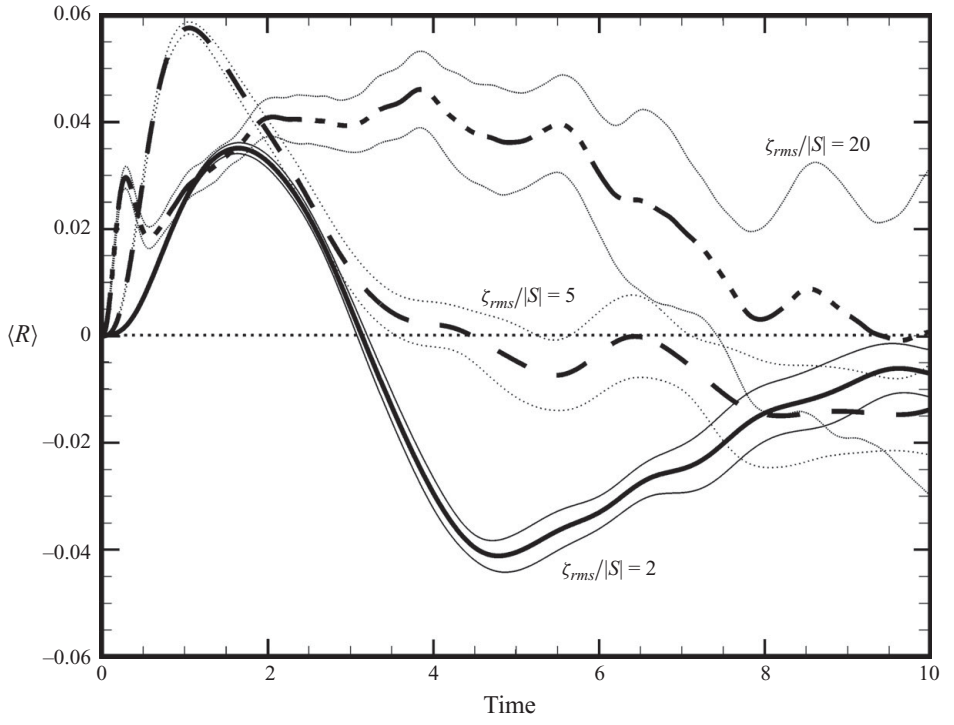

FIGURE 8. Time variation of the ensemble mean net Reynolds stress, $\langle R \rangle$, from experiments with $\zeta_{rms}/|S| = (2, 5, 20)$, represented by solid, dashed and dashed-dotted lines, respectively. Thin lines represent the 95 % confidence interval on the mean in each case.

the process of linear shearing acts in the sense of a net negative eddy viscosity on the disturbances, as suggested in § 2.2 and by Shepherd (1987).

4.1.3. *Variation of* $\zeta_{rms}/|S|$

A number of additional experiments were run with the nonlinear inviscid model in which the parameter, $\zeta_{rms}/|S|$ is varied. Figure 8 presents time series of the ensemble mean Reynolds stress, $\langle R \rangle$ with 95 % confidence limits from cases with $\zeta_{rms}/|S| = 2, 5, 20$. These may be compared with the results given in figure 3(a) for the reference case ($\zeta_{rms}/|S| = 10$). Each of these nonlinear experiments shows the development of positive Reynolds stress lasting over the first few advection time units. In the case of relatively weak nonlinearity ($\zeta_{rms}/|S| = 2$), this is followed by a statistically robust period of net negative Reynolds stress. Development of this negative viscosity regime is suppressed as the nonlinearity is increased ($\zeta_{rms}/|S| > 5$) and, for larger values of the parameter, the positive viscosity regime persists until nearly the end of simulations, at which point the spectral gap collapses.

These results may be interpreted in terms of the competition between finite-domain effects tending to produce negative eddy viscosity, as mentioned above, and the isotropizing tendency of eddy interactions. In every case there is an accumulation after some time of energy at the largest scales, due to the inverse cascade and shear-induced spectral transfers, and this produces a tendency for negative eddy viscosity. With $\zeta_{rms}/|S| = 2$ the opposing tendency associated with isotropization of higher wavenumbers is weak in comparison with the more nonlinear experiments, as is evident from inspection of Reynolds stress spectra (not shown). Consequently, there is

a period of negative eddy viscosity that follows the initial period of positive viscosity. Towards the end of the simulations, as the spectral gap is closed, the Reynolds stress in all the cases becomes variable and of indefinite sign.

Nonlinear interactions are seen to play an interesting double role with regard to the Reynolds stress in these simulations. On one hand, nonlinearity leads to isotropization of the smaller eddy scales, and so is essential for development of the positive viscosity regime. However, nonlinearity also produces the inverse cascade that leads to an accumulation of energy at the lowest wavenumbers, thus promoting development of a competing tendency to negative eddy viscosity through linear shearing. This may lead to an overall negative eddy viscosity if the tendency to restore isotropy at the higher eddy wavenumbers is sufficiently weak.

4.2. *Decaying simulations*

The sensitivity of the results presented above to the inclusion of explicit Laplacian friction was examined in a series of decaying simulations. All of the nonlinear inviscid simulations of § 4.1 were repeated with the viscosity, υ, chosen such that the grid Reynolds number, $Re_G \sim 4$–9, is sufficiently small to prevent the development of enstrophy equipartition (Bennett & Haidvogel 1983), but large enough to leave the energetic scales of motion largely undamped. Here $Re_G = \sqrt{2E|_{t=0}}/k_G\upsilon$ with $k_G = \sqrt{2}\pi/\Delta s$. Thus, in contrast to the inviscid calculations, there is no accumulation of grid-scale variance, and energy spectra roll off steeply at high wavenumbers. In this regard, the decaying experiments amount to an examination of the sensitivity of the inviscid results to the treatment of small-scale motions.

Results are presented from a case that makes use of the same ensemble of initial eddy vorticity fields as in the reference case ($\zeta_{rms}/|S| = 10$ at $t = 0$). The boundary condition, $\zeta = 0$, is imposed along the channel sidewalls so that there is zero tangential stress at the boundaries. An example of a vorticity field from one member of the ensemble for this experiment at $t = 1.1$ is presented in figure 1(*d*). This shows eddy structures that are similar to the inviscid case (figure 1*b*), but with much reduced fine-scale variation. Eddy kinetic energy spectra (figure 2*d*) undergo an evolution similar to that of the reference case, except for the high wavenumber tail.

Channel-averaged statistics from the decaying simulation are presented in figure 9. Due to the explicit viscous damping, the total kinetic energy of the ensemble decreases slowly (figure 9*b*), while the enstrophy undergoes a much more rapid and complete decay (figure 9*c*). The time variation of the ensemble mean Reynolds stress (figure 9*a*) resembles that of the reference case (figure 3*a*) with development of robust positive Reynolds stress, and an overall positive eddy viscosity. The eddy kinetic energy (figure 9*b*) decreases initially due to the Laplacian friction, but increases subsequently as energy is extracted from the zonal mean flow via the Reynolds stresses. This occurs while the overall energy decays monotonically. Towards the end of the simulation, as the dominant eddy scale approaches that of the channel, the mean Reynolds stress changes sign and the eddy energy also decreases.

Results of this decaying simulation are thus essentially unchanged from the inviscid reference experiment with respect to the net Reynolds stress and eddy viscosity. Additional decaying simulations were run with initial conditions for which $\zeta_{rms}/|S| = (2, 5, 20)$ at $t = 0$. The time variation of the net Reynolds stress in these simulations (figure available as supplementary material at journals.cambridge.org/flm) is similar to the corresponding inviscid cases presented in figure 8. Overall, the decaying simulations indicate that the Reynolds stress is insensitive to the frictional suppression of poorly resolved, grid-scale motions. This is understandable as the

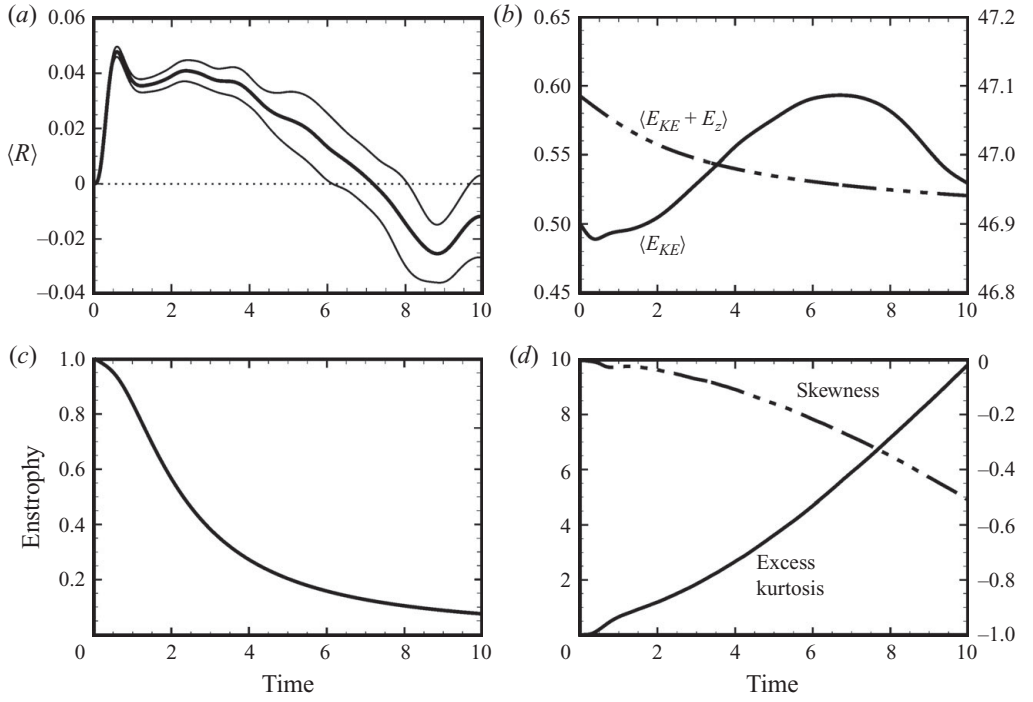

FIGURE 9. Ensemble mean results from a decaying simulation with $\zeta_{rms}/|S| = 10$ at $t = 0$. (*a*) Time variation of the net Reynolds stress, $\langle R \rangle$, with 95% confidence interval. (*b*) Total kinetic energy, $\langle E_{KE} + E_Z \rangle$ (right scale), and eddy kinetic energy, $\langle E_{KE} \rangle$ (left scale). (*c*) Enstrophy normalized by value at $t = 0$. (*d*) Excess kurtosis (left scale), and skewness (right scale).

energy-containing well-resolved scales of motion are effective at restoring isotropy at higher eddy wavenumbers.

In contrast to the inviscid evolution, inclusion of explicit friction is associated with development of markedly non-Gaussian vorticity distributions. In particular, the excess kurtosis increases monotonically from its initial Gaussian value of zero (figure 9*d*) as the vorticity becomes increasingly concentrated into a collection of discrete vortices (McWilliams 1984). Figures 9(*a*) and 9(*d*) indicate that the positive eddy viscosity regime persists until the spectral gap collapses, even as the vorticity kurtosis increases.

While the formation of coherent vortices is well known, a less familiar property of sheared decaying turbulence is development of skewness in the vorticity distribution (figure 9*d*). This is associated with the destruction of coherent vortices that are of opposite sign to the vorticity of the background shear. These vortices are elongated and homogenized by the shear flow (cf. Marcus 1990; Toh *et al.* 1991), such that ultimately the only surviving coherent vortices have the sign of the background vorticity. These coherent vortices move within a sea of weak oppositely signed vorticity and tend to assume an elliptical shape with semimajor axes aligned with the background flow, consistent with studies on the stability of two-dimensional vortices in shear (Nycander 1995). Such a state is achieved following an extended integration. An example, drawn from a decaying run at $t = 54$, is presented in figure 10. As the majority of the coherent vortices are negative, the skewness of this field is -3.7, while the kurtosis is

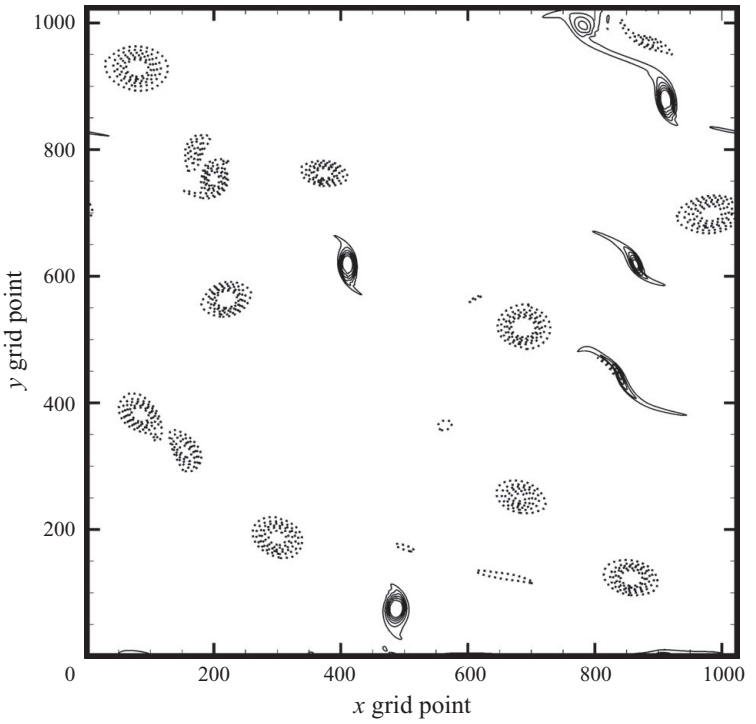

FIGURE 10. Eddy vorticity field at $t = 54$ from a decaying run on a 1024×1024 grid. The contour interval is $0.1\,\zeta_{rms}$ based on the r.m.s. vorticity at $t = 0$. Negative contours are dotted, and the zero contour has been suppressed.

40.1. The time scale for such a large skewness to emerge is long in comparison to the time required to close the spectral gap.

5. Summary

Direct numerical simulations have been conducted to examine the sign of the eddy viscosity for homogeneous isotropic eddies in the presence of a large-scale shear flow. The experiments consist of ensembles of initial-value-problems in which small-scale isotropic disturbances are superposed on a plane Couette flow in a periodic channel. The simulations show the emergence of a robust positive viscosity phenomenology in both inviscid and decaying turbulence. The positive viscosity regime develops within the first few eddy-turnaround time units following release of the initial conditions, while effects associated with the finite scale of the channel domain are unimportant. Based on these results, the main conclusion of this study is that, in the presence of a spectral gap, the eddy viscosity of initially isotropic two-dimensional turbulence is positive.

Reynolds stress spectra were examined to elucidate the process by which this occurs. These spectra show that linear shearing produces counter-balancing tendencies for positive and negative eddy viscosity at low and high eddy wavenumbers, respectively. This process alone produces zero net stress for an isotropic homogeneous field of eddies. The inclusion of nonlinear eddy interactions produces a tendency to restore isotropy that is most efficient at higher eddy wavenumbers. This partially suppresses

the negative eddy viscosity contribution from linear shearing, leading to an overall positive eddy viscosity.

The positive eddy viscosity regime is maintained as the scale of the disturbances increases due to the combined effects of the inverse cascade and shear-induced spectral transfers. Eventually though, effects of the finite-domain size become manifest and the process of linear shearing produces a tendency for negative eddy viscosity. The resulting stress then depends on the time-dependent balance between the competing processes of linear shearing and nonlinear isotropization.

Supplementary figure available at journals.cambridge.org/flm.

REFERENCES

Arakawa, A. 1966 Computational design for long term numerical integration of the equations of fluid motion: two-dimensional incompressible flow. Part 1. *J. Comput. Phys.* **1**, 119–143.

Bennett, A. F. & Haidvogel, D. B. 1983 Low-resolution numerical simulation of decaying two-dimensional turbulence. *J. Atmos. Sci.* **40**, 738–748.

Benzi, R., Manfroi, A. J. & Vergassola, M. 1996 Vorticity selection in large-scale two-dimensional flow. *Europhys. Lett.* 36, 367–371.

Chaves, M. & Gama, S. 2000 Time evolution of the eddy viscosity in two-dimensional Navier–Stokes flow. *Phys. Rev.* E **61**, 2118–2120.

Chen, S., Ecke, R. E., Eyink, G. L., Rivera, M., Wan, M. & Xiao, Z. 2006 Physical mechanism of the two-dimensional inverse energy cascade. *Phys. Rev. Lett.* **96**, 084502.

Cummins, P. F. & Holloway, G. 1994 On eddy-topographic stress representation. *J. Phys. Oceanogr.* 24, 700–706.

Eyink, G. L. 2006 A turbulent constitutive law for the two-dimensional inverse energy cascade. *J. Fluid Mech.* **549**, 191–214.

Fjortoft, R. 1953 On the changes in the spectral distribution of kinetic energy for two dimensional, nondivergent flow. *Tellus* **5**, 225–230.

Fox, D. G. & Orszag, S. A. 1973 Inviscid dynamics of two-dimensional turbulence. *Phys. Fluids* **16**, 169–171.

Gama, S., Vergassola, M. & Frisch, U. 1994 Negative eddy viscosity in isotropically forced two-dimensional flow: linear and nonlinear dynamics. *J. Fluid Mech.* **260**, 95–126.

Herring, J. R. 1975 Theory of two-dimensional anisotropic turbulence. *J. Atmos. Sci.* **32**, 2254–2271.

Holland, W. R. 1978 The role of mesoscale eddies in the general circulation of the ocean – numerical experiments using a wind-driven quasi-geostrophic model. *J. Phys. Oceanogr.* **8**, 363–392.

Holloway, G. 1989 Subgridscale representation. In *Oceanic Circulation Models: Combining Data and Dynamics* (ed. D. L. T. Anderson & J. Willebrand), pp. 513–593. Kluwer, 605 pp.

Holloway, G. 2010 Eddy stress in sheared 2D flow. *J. Turbulence* **11**, (in press).

Kraichnan, R. H. 1967 Inertial ranges in two-dimensional turbulence. *Phys. Fluids* **10**, 1417–1423.

Kraichnan, R. H. 1976 Eddy viscosity in two and three dimensions. *J. Atmos. Sci.* **33**, 1521–1536.

Marcus, P. S. 1990 Vortex dynamics in a shearing zonal flow. *J. Fluid Mech.* **215**, 393–430.

McWilliams, J. C. 1984 The emergence of isolated coherent vortices in turbulent flow. *J. Fluid Mech.* **146**, 21–43.

McWilliams, J. C. & Chow, J. H. S. 1981 Equilibrium geostrophic turbulence. I. A reference solution in a beta-plane channel. *J. Phys. Oceanogr.* **11**, 921–949.

Nycander, J. 1995 Existence and stability of stationary vortices in a uniform shear flow. *J. Fluid Mech.* **287**, 119–132.

Salmon, R. 1998 *Lectures on Geophysical Fluid Dynamics*. Oxford University Press, 378 pp.

Shepherd, T. G. 1985 Time-development of small disturbances to plane Couette flow. *J. Atmos. Sci.* **42**, 1868–1871.

Shepherd, T. G. 1987 Rossby waves and two-dimensional turbulence in a large-scale zonal jet. *J. Fluid Mech.* **183**, 467–509.

Sommeria, J. 1986 Experimental study of the two-dimensional inverse energy cascade in a square box. *J. Fluid Mech.* **170**, 139–168.

Starr, V. P. 1968 *Physics of Negative Viscosity Phenomena.* McGraw-Hill, 256 pp.

von Storch, H. & Zwiers, F. W. 1999 *Statistical Analysis in Climate Research.* Cambridge University Press, 484 pp.

Swarztrauber, P. & Sweet, R. 1975 Efficient FORTRAN subprograms for the solution of elliptic equations. *Tech. Rep.* TN/IA-109. NCAR, 138 pp.

Tabeling, P. 2002 Two-dimensional turbulence: a physicist approach. *Phys. Rep.* **362**, 1–62.

Toh, S., Ohkitani, K. & Yamada, M. 1991 Enstrophy and momentum fluxes in two-dimensional shear flow turbulence. *Physica* D **51**, 569–578.

Wang, J. & Vallis, G. K. 1994 Emergence of Fofonoff states in inviscid and viscous ocean circulation models. *J. Mar. Res.* **52**, 83–127.